RSC Advances

This is an *Accepted Manuscript*, which has been through the Royal Society of Chemistry peer review process and has been accepted for publication.

Accepted Manuscripts are published online shortly after acceptance, before technical editing, formatting and proof reading. Using this free service, authors can make their results available to the community, in citable form, before we publish the edited article. This *Accepted Manuscript* will be replaced by the edited, formatted and paginated article as soon as this is available.

You can find more information about *Accepted Manuscripts* in the Information for Authors.

Please note that technical editing may introduce minor changes to the text and/or graphics, which may alter content. The journal's standard Terms & Conditions and the Ethical guidelines still apply. In no event shall the Royal Society of Chemistry be held responsible for any errors or omissions in this *Accepted Manuscript* or any consequences arising from the use of any information it contains.

ROYAL SOCIETY OF CHEMISTRY

www.rsc.org/advances

Hydrocarbon degradation and separation of bilge water via a novel TiO_2-HNTs/PVDF-based photocatalytic membrane reactor (PMR)

A. Moslehyani,[a,b], A. F. Ismail, [a,b,]*, M. H. D. Othman,[a,b], T. Matsuura [a,c]

[a] *Advanced Membrane Technology Research Centre (AMTEC), Universiti Teknologi Malaysia, 81310 UTM Skudai, Johor Darul Ta'zim, Malaysia*
[b] *Faculty of Petroleum & Renewable Energy Engineering, Universiti Teknologi Malaysia, 81310 UTM Skudai, Johor Darul Ta'zim, Malaysia*
[c] *Department of Chemical and Biological Engineering, University of Ottawa, 161 Louis Pasteur St., Ottawa, ON K1N 6N5, Canada*
*Corresponding author: afauzi@utm.my; fauzi.ismail@gmail.com, Tel: +607-5535592, Fax: +607-55355925

Abstract

This paper focuses on the potential of a novel flat sheet nanocomposite titanium dioxide (TiO_2)-halloysite nanotubes (HNTs)/polyvinylidene fluoride (PVDF) membrane as a photocatalytic separator in the photocatalytic membrane reactor (PMR). The photocatalytic nanocomposite membrane acted the roles of both degradation and separation for the bilge water. Both TiO_2-HNTs photocatalyst and photocatalytic nanocomposite membranes were characterized by thermal gravimetric analysis (TGA), Fourier transform infrared (FTIR), X-ray diffraction (XRD), and field emission scanning electron microscopy (FESEM) combined energy dispersive X-ray (EDX). The hydrocarbon degradation and removal efficiency of the PMR was evaluated by gas chromatography mass spectroscopy (GC-MS). It was found that 99.9 % of hydrocarbons were removed by the PMR within 8 h, which is likely due to uniform distribution and high effectiveness of TiO_2-HNTs photocatalyst in the PVDF polymer matrix. The TiO_2 leaching from the nanocomposite membrane during the membrane permeation was analyzed by using flame atomic adsorption spectrophotometer (AAS), which recorded 1.0 ppb of TiO_2 leaching in the permeate tank.

Keywords: PMR, TiO_2-HNTs, PVDF, photodegradation, nanocomposite membrane

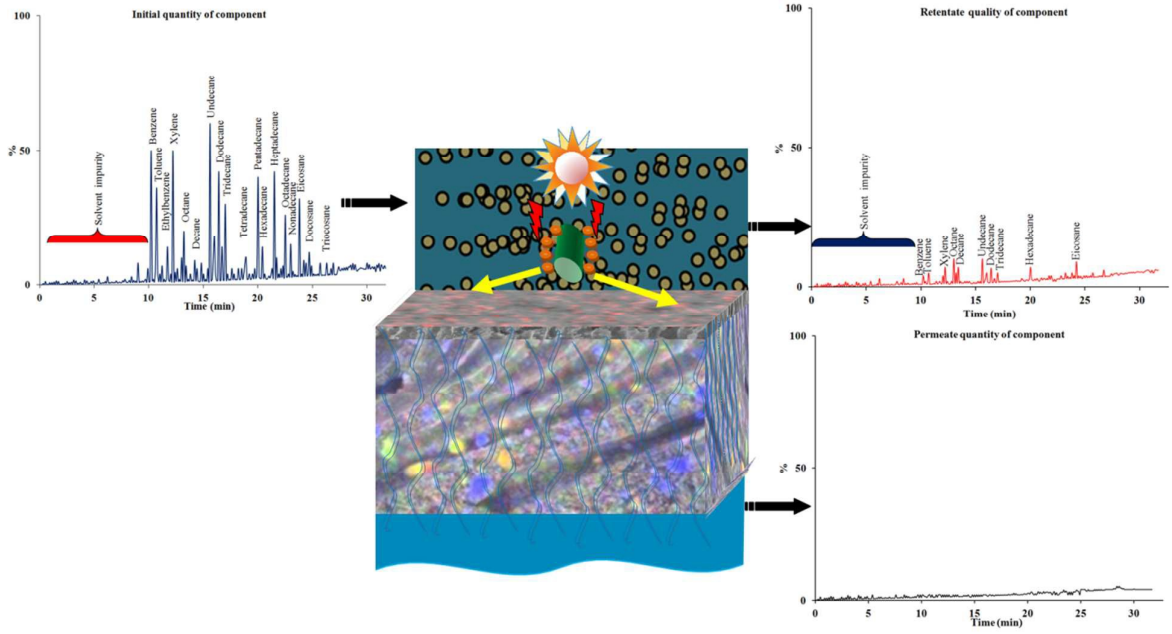

RSC Advances Accepted Manuscript

1. Introduction

Bilge water is composed of corrosive mixture of different hydrocarbons (HC) from engine oil and fuel tank of ships. Bilge water is commonly discharged to the sea without a proper treatment, which contributing to a major pollution in the seawater and affecting marine ecosystems and human health [1]. International Maritime Organization (IMO) has set the maximum oil content for the ship discharge should not be more than 15 ppm according to MARPOL 73/78 convention [1, 2]. This means that an affective on-board bilge treatment is necessary for all ships [3].

Oil-in-water separators are currently being used to treat bilge water in the ships [4]. However, the main weaknesses of this approach are the presence of small organic particles in the discharged stream [5] and the extremely long time required for the separation process. In addition, normal separation techniques such as ultrafiltration, nanofiltration and reverse osmosis (RO) [6] are only able to separate organic compounds from water instead of degrade toxic pollutants. Previously, biological degradation technique has been used to degrade hydrocarbon compounds in bilge water [7-9], where, bioreactor system containing microorganisms was applied to degrade hydrocarbons and treat more than 300 m^3 bilge water each month [1]. More recently, the efficiency of bio-degradation via different types of bacteria suspension in bilge water has also been studied [10]. Those bacteria were degrading more than 70% of hexane and more than 90% of arenes [11]. Furthermore, degradation of hydrocarbon compounds in bilge water was possible to be enhanced by applying cyclo-dextrins to increase their solubility in water (e.g. after 120 h of bilge treatment just 15% of hexadecane was un-degraded while 43% was un-degraded without cyclo-dextrin applying) [12].

Recently, advanced oxidation processes (AOPs) have been shown high performance for degradation of organic compounds to the harmless materials under sensible condition [13, 14,15]. Accordingly, AOPs by the use of TiO_2 photocatalyst has gained more interest [16] since TiO_2 is regarded as an acceptable and cheap photocatalyst material [17,18]. In order to treat the bilge water samples, photocatalytic reactor combined with membrane filtration has been proposed in order to achieve total decomposition [19] and purification of the oily wastewater [20] by incorporating TiO_2 in the polymeric membrane.

To prevent the agglomeration of TiO_2 nanoparticles in the polymer maxtrix, TiO_2 has been supported by nanoparticles or nanotubes such as carbon nanotubes [23], graphene [24] and magnetic particles [25]. Recently, halloysite nanotubes (HNTs) which are made from aluminosilicate clay exhibited high potential as a supporting photocatalyst [26] due to their nano-tubular structure, presence of hydroxyl groups [27] and different functional groups at the inside and outside surface. Thus, immobilizing the TiO_2 nanoparticles on the HNTs surface was reported as an effective way to prevent aggregation [28]. In addition, HNTs showed high stability, ease of disposal or reusability, high resistance against organic solvents [28] and cheaper price than carbon nanotubes (CNTs) [29]. HNTs can be used as a support layer for the TiO_2 nanoparticles [30], due to the prence of hydroxyl radicals at its surface. The immobilizing of TiO_2 on the HNTs surfaces has shown a great potential for adsorption and photocatalytic activities, which may enhance efficiency for photocatalytic degradation of different contaminants [31].

Consequently, immobilization of TiO_2-HNTs photocatalyst and fabrication of PVDF/TiO_2-HNTs photocatalytic membrane submerged in the PMR was focused by this study. The

RSC Advances Accepted Manuscript

performance of the photocatalytic membrane and PMR were examined and analyzed for better understanding of this particular PMR system.

2. Experiment

2.1. Materials

Polyvinylidene fluoride (PVDF) Solef 6012 in pellet from Solvay Advanced Polymers, dimethylacetamide (DMAc, >99.5%) from Merck, were used as polymer and solvent, respectively. Halloysite nanotubes (HNTs) clay with inner tube diameter of 5-15 nm was purchased from Sigma Aldrich. N-β-(aminoethyl)-ɣ-aminopropyltrimethoxy silane (AEAPTMS) from Merck, toluene and tetra hydro furane (THF) from QReC was used for TiO_2-HNTs immobilization. Titanium dioxide (TiO_2) P25 nanoparticles (surface area of 50±15 m^2/g) were purchased from Degussa.

2.2. TiO_2-HNTs photocatalyst preparation

TiO_2 was chemically immobilized to the HNTs surface via AEAPTMS by the following procedure; firstly 10 g of AEAPTMS was dissolved in 100 mL toluene by sonication and then 10 g HNTs and 10 g TiO_2 were poured into the solution and refluxed at 95 ^oC for 24 h under rigorous stirring. Then, the product TiO_2-HNTs were washed by centrifuging consecutively with 500 mL THF and 500 mL distilled water. The TiO_2-HNTs were kept in an oven at 85 ^oC for 48 h for drying purposes. The schematic diagram of this process is illustrated in Fig. 1.

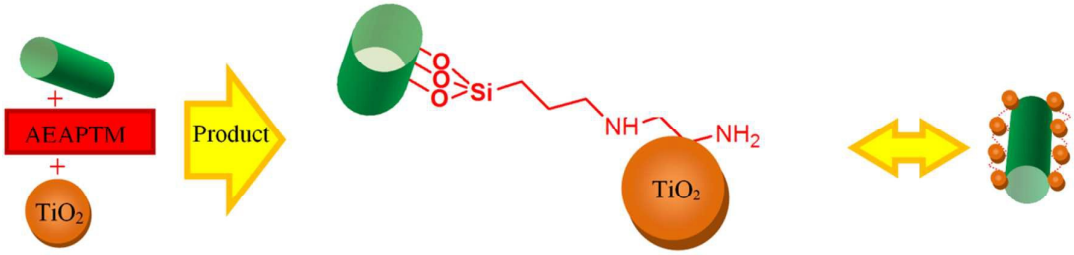

Fig. 1. Schematic diagram of the formation of TiO_2-HNTs photocatalyst

2.3. Nanocomposite membrane production

Neat PVDF and PVDF/TiO_2-HNTs nanocomposite membrane denoted as M1 and M2, respectively, were fabricated via the wet phase-inversion technique. The casting solution composition was 18 wt% PVDF and 82 wt% DMAc for M1 and 18 wt% PVDF, 81 wt% DMAc and 1 wt%TiO_2-HNTs for M2. In particular, for M2 the following casting procedure was adopted to disperse the nanoparticles uniformly. Firstly, TiO_2-HNTs nanoparticles were added into DMAc and sonicated for 6 h before PVDF was poured slowly under vigorous agitation. The mixture was kept agitated for 24 h, and then sonicated at 65 ^oC for 4 h to remove air bubbles. The prepared dope was cast onto a glass plate by a hand-casting knife to a thickness of 250 µm, prior to immersion into distilled water for 3 days, where the cast film was solidified and peeled off the glass plate spontaneously. Then, the membrane was immersed in the 2:1 mixture of methanol:distilled water for 5 h.

RSC Advances Accepted Manuscript

2.4. Nanocomposite membrane characterization

Fourier transform infrared (FTIR) analysis of HNTs and TiO_2-HNTs was performed at 2 cm^{-1} resolution by FTIR equipment (Thermo Nicolet Corporation, USA) in a range of 400–4000 cm^{-1} using KBr pellets. Typically, 64 scans were signal-averaged to reduce spectral noise. Thermal gravimetric analysis (TGA) for the neat PVDF and PVDF/TiO_2-HNTs composite membrane was carried out using a TG-DTA, DT-40 system (Shimadzu, Japan), in which 3 mg of each membrane sample was heated (from 0 to 800 ^oC at the rate 10 ^oC/min) under nitrogen flow. XRD analysis was achieved for the photocatalyst, neat PVDF (M1) and nanocomposite (M2) membrane (at 50 mA and 50 kV). The cross-section and the top surface of the membrane were observed by field emission scanning electron microscope (FESEM, Jeol JSM 6701-F) combined with energy dispersive X-ray (EDX- Jeol JED-2300F). The water contact angle was measured by contact angle analyzer (model IMC-159D by IMOTO Machinery Co. Ltd.) by dropping of 5 µl de-ionized water to the membrane surface. The mean pore size, μ_p (nm), was determined from the atomic force microscopy (AFM) image of the membrane surface by the method developed by Singh *et al,* [32]. In membrane filtration experiments, permeation flux was measured gravimetrically by Eq. (1):

$$J = \frac{V}{A \times t} \qquad \text{Eq. (1)}$$

where volume of permeate was V (L), membrane effective area was A (m^2), and sampling time was t (h). Bilge rejection percentage R(%) was calculated by Eq (2):

$$R(\%) = 1 - (\frac{C_P}{C_F}) \times 100 \qquad \text{Eq. (2)}$$

where C_P (ppm) is bilge concentration in permeate and C_F (ppm) is the bilge concentration in the PMR, which remained almost the same during the entire PMR operation. Flux decline, FD_t (%) was calculated by Eq. (3):

$$FD_t(\%) = (1 - \frac{J_{P,t}}{J_{P,i}}) \times 100 \qquad \text{Eq. (3)}$$

where $J_{p,t}$ was the flux at time t ($Lm^{-2}h^{-1}$), typically t is equal to 1 h, and $J_{p,i}$ was the initial flux (Lm^{-2} h^{-1}), at t = 0 h from the initiation of filtration. Flux recovery has been caculated by the Eq. (4)

$$R_{FR} = \frac{J_{t2}}{J_{t1}} \times 100 \qquad \text{Eq. (3)}$$

where J_{t2} was the flux at second time t ($Lm^{-2}h^{-1}$) atfter membrane back washing, typically t is equal to 1 h, and J_{t1} was the flux at first time (Lm^{-2} h^{-1}), at typically t equal to 1 h from the initiation of filtration.

RSC Advances Accepted Manuscript

2.5 Photocatalytic degradation and filtration measurement

The bilge water was obtained from one of the Eastern Malaysian oil tankers. The physical specifications of bilge water are listed in Table 1.

Table 1
Characterization of bilge wastewater

Parameters	Data
Concentration of hydrocarbons in bilge water at initial time	200 (ppm)
Viscosity of bilge water	1.21 (centipoise)
initial bilge droplet in PMR	0.80 (μm)
Retentate bilge droplet in PMR	1.84 (μm)

The membrane was immersed in the PMR, then bilge water sample was transferred from the feed tank to the PMR for the following total 8 h operation. Firstly, bilge water was irradiated by UVC light in the presence of the membrane for 6 h in the switched-off pump (peristaltic pump on the permeate side) condition. During the last 2 h the pump was switched-on for the filtration purposes and the permeate side pressure was set at different subatmospheric pressures (i.e. -0.2, -0.4, -0.6 and -0.8 bar gauge). Since the pressure of PMR is atmospheric pressure (0 bar gauge), the transmembrane pressure difference was set to 0.2, 0.4, 0.6 and 0.8 bar. The hydrocarbons in PMR, retentate and permeate were identified and quantified by GC-MS (Agilent system equipped with HP.5-MS column; retention time, 33 min) analysis. For this purpose 10 mL of samples were collected each 30 min during the entire running period (8 h). Prior to the GC-MS analysis, liquid-liquid extraction (LLE) technique was carried out to transfer hydrocarbons to organic solvent.

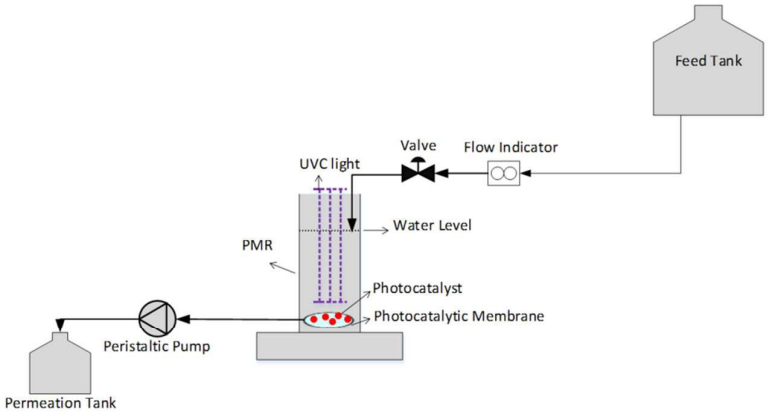

Fig. 2. Illustration of PMR for bilge water degradation and separation

3. Discussion

3.1 FTIR analysis of photocatalyst TiO_2-HNTs

Fig. 3 displays the FTIR spectra of (i) raw HNTs and (ii) immobilized TiO_2-HNTs. In TiO_2-HNTs new peaks appeared at 533 and at 465 cm^{-1}, which were corresponded to Al-O-Si and Si-O-Si, respectively. Hydroxyl group signal was also detected at 912 cm^{-1} for TiO_2-HNTs sample, in contrast to the original HNTs. The 1007 cm^{-1} signal of Si-O broad stretching band shifted to 1029 cm^{-1} due to the presence of hydrogen bonding between outer HNTs surface

RSC Advances Accepted Manuscript

and TiO_2 nanoparticles. The position of other peaks in HNTs remained unchanged, indicating that the basic structure of HNTs was retained, which also was in agreement with the literature [27].

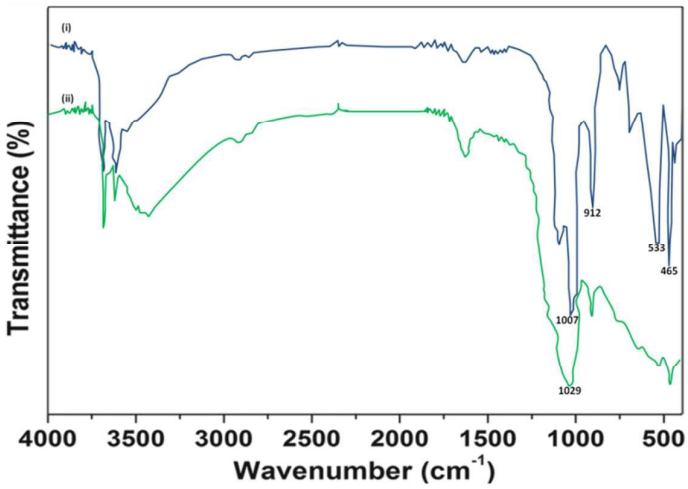

Fig. 3. FTIR spectra of (i) HNTs and (ii) TiO_2- HNTs

3.2 Photocatalytic nanocomposite membrane characteristics

3.2.1 Thermo gravimetric analysis of photocatalytic nanocomposite membrane

The thermal characteristics of M1 and M2 were shown by Fig. 4. The thermal decomposition (T_d) of M2 was higher than M1, i.e. T_d of 338.67 ^oC for M1 has moved to 369.73 ^oC for M2. This proved that the addition of TiO_2-HNTs into the PVDF polymer matrix has increased the thermal stability of M2. Moreover, T_g of PVDF increased by the incorporation of TiO_2-HNTs due to the interaction between the macromolecular chain and the polar group at the immobilized TiO_2-HNTs surface, which is in agreement with the report in the literature[33].

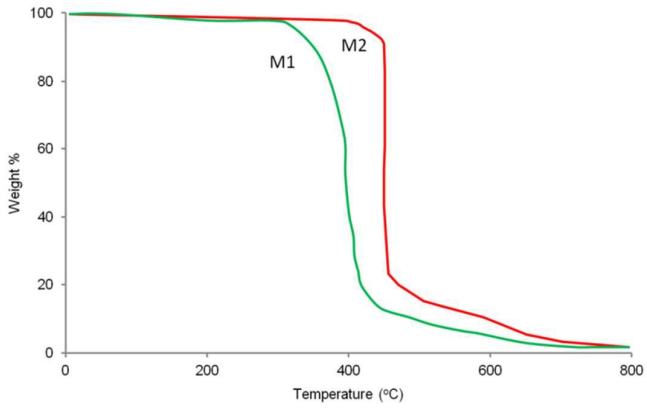

Fig. 4. Thermo gravimetric curves of M1(green) and M2 (red)

3.2.2 X-ray diffraction patterns

Fig. 5 shows the X-ray diffraction (XRD) characteristics for (a) TiO_2-HNTs , (b) M1 and (c) M2. TiO_2-HNTs showed the 3 crystalline spectra at 2θ of 13.6, 28.3, 45.46, 56.1, 62.3, 64.1 and 72.64^o, which were also found by the other studies [31]. M2 also possessed crystalline patterns at 2θ of 27.61, 45.46, 56.10, 62.30, 64.10 and 72.31^o, which are almost the same as

RSC Advances Accepted Manuscript

TiO_2-HNTs. This probably indicates the tetrabutyl titanate formation by TiO_2 nanoparticles with hydrolytic reaction in the M2 [26, 31]. Additionally, the peaks at 20.61 and 23.47° in M1 are regarded as the diffractions at 020 and 021 planes, respectively, of the α-phase structure of PVDF. The peak at 23.41° in (c) comes from the diffraction in the 110 and 200 planes of the β-phase structure of PVDF. It shows clearly the TiO_2-HNTs were dispersed successfully to the PVDF matrix, which has affected the PVDF crystal structure (transition from α-crystalline phase to β-crystalline phase) in the M2 as it was also observed by other researchers [33].

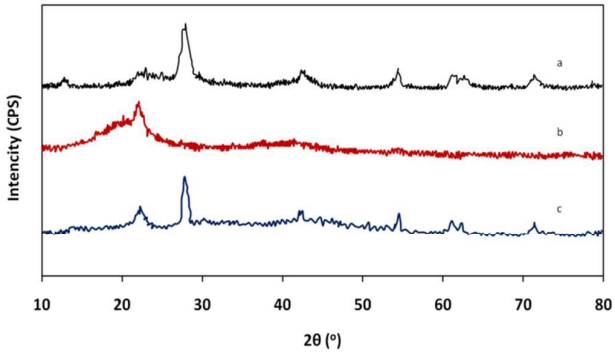

Fig. 5. XRD curves of (a) TiO_2-HNTs photocatalyst, (b) M1 and (c) M2

3.2.3 Membrane morphology

The presences of elements in M1and M2 have been confirmed by EDX analysis and listed in Table 2. The surfaces of both membranes have more than 60 wt% of F element which comes from PVDF, however, M2 shows relatively lower wt% compared to M1. On the other hand, Ti of 0.6 wt% is present in the M2 surface due to incorporation of TiO_2-HNTs. Another two elements (i.e. Si and Al) are the evidence for the presence of HNTs in M2. The element mapping from FESEM images in the BSE mode is illustrated in Fig. 6a and b1 for M1 and M2, respectively. Overall cross-sectional morphology and element mapping of M2 (Fig. 6b1 and 6b2) shows the presence of Ti (from TiO_2) and Si, Al (from HNTs) over the entire cross-section. As well, a longer finger-like structure was formed in M2 compared to M1 (Fig. 6(a)), suggesting enhanced permeate flux of M2. Fig. 6b2 was showing the uniform TiO_2 dispersion over the membrane surface, which is marked particularly. This uniform distribution of TiO_2 immobilization on the HNTs surface is believed that due to the sonication process that has been performed prior to adding PVDF polymer [33].

Table 2
EDX element composition detection

Membrane	Elements (wt%)				
	F	Ti	Si	Al	Others
M1	62.23	0.00	0.00	0.00	37.77
M2	60.31	0.60	0.20	0.07	38.82

RSC Advances Accepted Manuscript

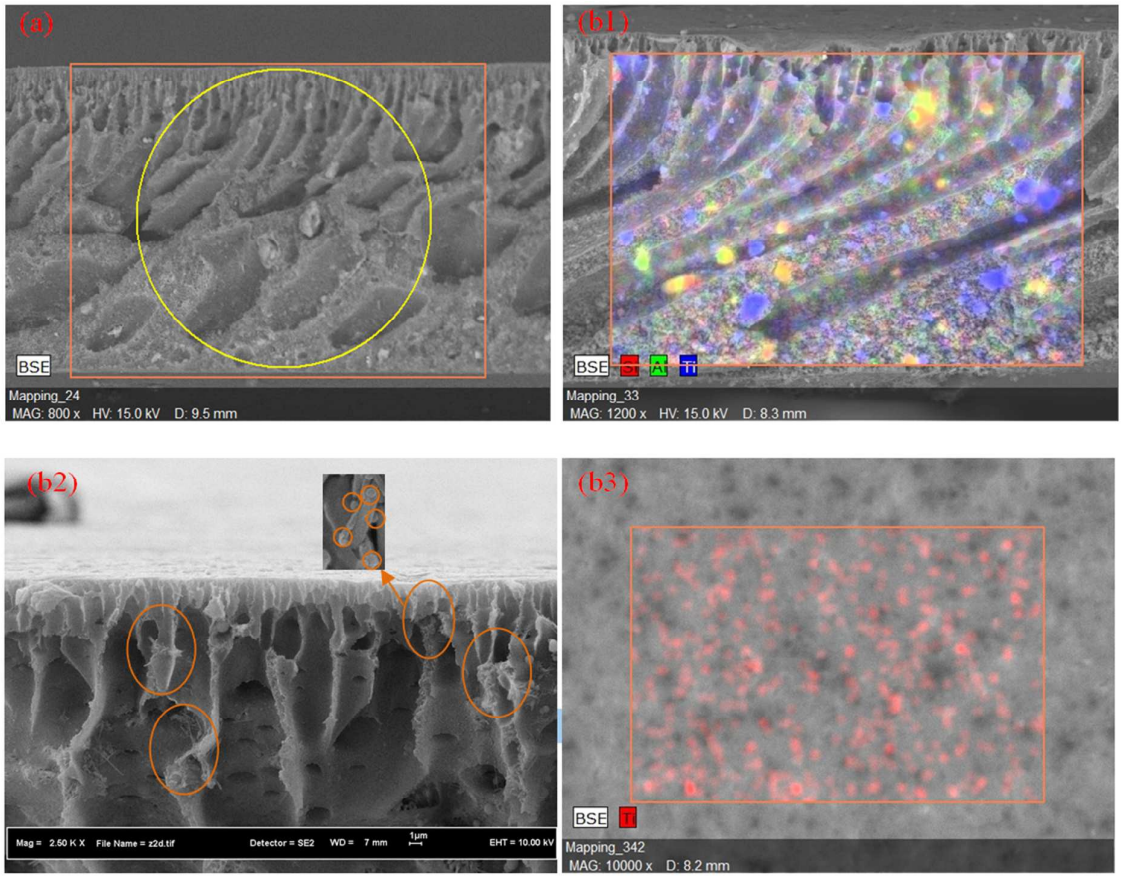

Fig. 6. FESEM images of (BSE mode) for (a) M1, (b1and b2) M2 cross-section and (b3) M2 top surface

Other M1 and M2 properties such as mean pore size, contact angel, tensile strength and elongation at break are summarized in Table 3. From Table 3, the mean pore size and the contact angle decreased by the incorporation of TiO_2-HNTs. Thus, the membrane surface became more hydrophilic. The stated results for contact angel and mean pore size were shown a promising specification for M2, which may affected in the membrane performance. The tensile strength increased and elongation at break decreased by the incorporation of TiO_2-HNTs due to suppression of macro voids as well as the interaction among inorganic photocatalyst and polymer, according to Li Yun *et al.* [31].

Table 3 Mean pore size, contact angle, tensile strength and elongation at break of the membranes

Membrane types	Mean pore size, (nm)	Contact angel (^{o})	Tensile strength (MPa)	Elongation at break (%)
M1	52±39	78.50±3.1	1.63	159.39
M2	47±12	46.36±1.4	2.19	125.74

RSC Advances Accepted Manuscript

3.3 Performance of membrane in PMR

3.3.1 Effect of UV photodegradation of hydrocarbons

The performance of the membrane in terms of photodegradation for bilge water was achieved by GC-MS analysis. As it mentioned earlier, hydrocarbons in bilge water (e.g. arenes) are highly toxic, hence, their degradation is necessary before discharging to environment. Accordingly, the photocatalytic degradation was conducted for 8 h via UVC irradiating to the submerged membrane surface.

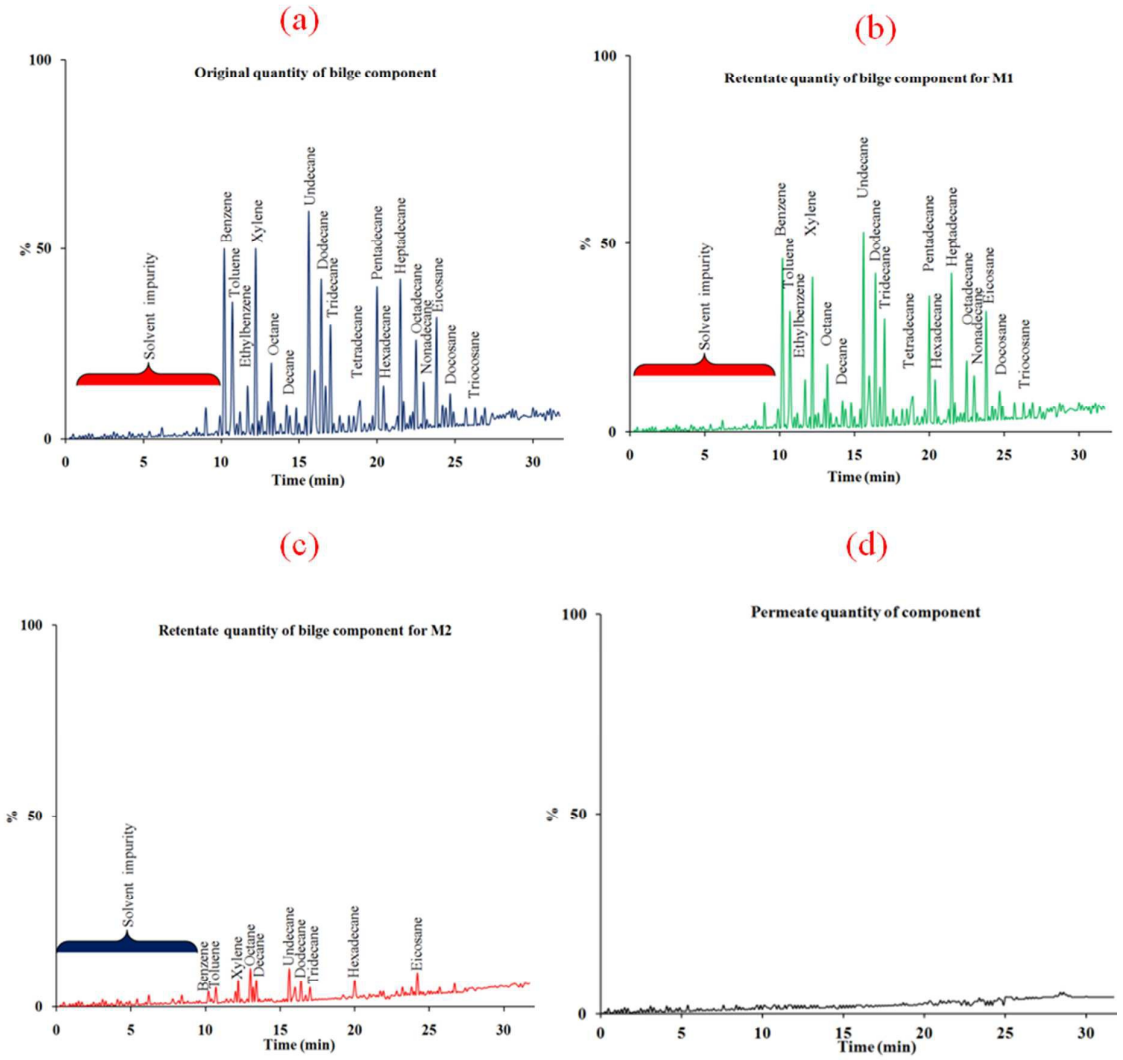

Fig. 7. GCMS chromatograms quantity of component for (a) original bilge water in feed tank, (b) bilge water retentate after 8 h UV irradiation in PMR on the submerged M1 surface, (c) bilge water retentate after 8 h UV irradiation in PMR on the submerged M2 surface, and (d) permeate water for M1 and M2

Fig. 7 depicts four different GC spectra; (a) original bilge water in the feed tank, (b) bilge water retentate after 8 h UV irradiation in PMR on the submerged M1 surface, (c) bilge water retentate after 8 h UV irradiation in PMR on the submerged M2 surface, and (d) represents

RSC Advances Accepted Manuscript

the permeate from M1 and M2, at 0.8 bar transmembrane pressure difference. Figs. 7(a) and (b) are practically the same, indicating that no photodegradation took place when M1 was installed in PMR. On the other hand, in Fig. 7(c) many peaks appearing in Fig. 7(a) were either completely removed or reduced in their intensities, indicating that photodegradation took place at the surface of M2. The total area of the peaks was reduced more than 90% from Fig. 7(a) to 7(c). Figure 7(d) represents permeate from M1 and M2. It seems hydrocarbons could be effectively removed by filtration by both M1 and M2. pH of each sample was also measured. The pH values for the samples that correspond to Figs. 7(a), (b), (c) and (d) were 8.56, 5.98, 4.79 and 6.37, respectively. This indicates that acidic substances are formed by hydrocarbon degradation and they are removed by membrane filtration.

3.4.2 Effectiveness of membrane separation

3.4.1 Permeation flux

As mentioned earlier, after 6 h of UV irradiation in the PMR the peristaltic pump was turned on to collect permeate from the membrane for the following 2 h , during which period the permeate flux, decreased gradually due to membrane fouling.
The permeation flux (J) obtained after 1 h filtration operation (t = 1 h) is shown in Fig. 8 for 4 different transmembrane pressure differences (0.2 - 0.8 bar).,In the figure, M2 showed higher fluxes than M1, due to M2's higher surface hydrophilicity (Table 3) and larger number of finger-like pores (Fig. 6). The flux increased with an increase in the transmembrane pressure difference, but the increase was not necessarily proportional to the transmembrane pressure difference, which is typical to the gel layer formation at the membrane surface.

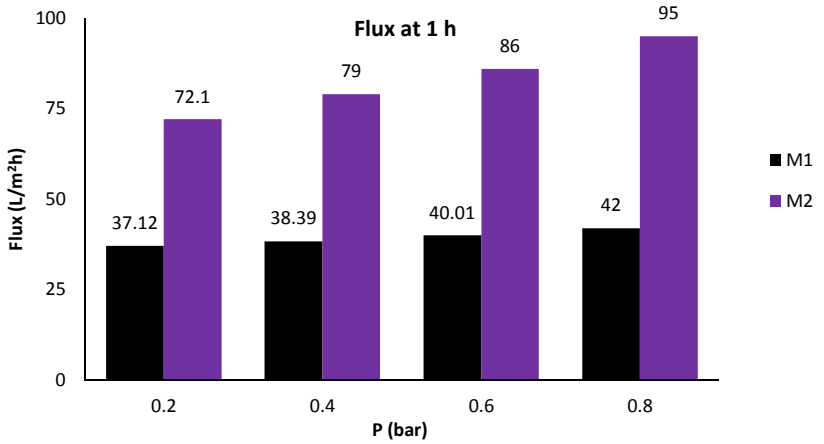

Fig. 8. Permeation flux as a function of transmembrane pressure difference for M1 (black) and M2 (violet)

3.4.2 Anti-fouling behavior

Fig. 9 represents fouling of the fabricated membranes at 1 h of filtration for all operating pressures, which was calculated based on Eq. (3). From Fig. 9, M1's FD is greater thn M2, possibly because of more hydrophilic nature of M2's membrane surface, which prevents deposition of oily foulant. Regarding M2, FD becomes greater as the transmembrane pressure difference increases. A plausible explanation for this effect is as follows. Generally, membrane fouling is caused by the following two parameters; i) pore blocking [34], and ii)

RSC Advances Accepted Manuscript

concentration polarization and deposition of foulant at the membrane surface [35]. Pore blocking takes place in the earlier stage of filtration and concentration polarization and oil layer deposition become more severe at the later stage. The FD of membranes is more significant at the higher pressure, which can be related to the mechanism of pore blocking as reported by Vela *et al.* in 2008 [34]. On the other hand, the increase in the fluid movement at higher transmembrane pressure difference may cause enhanced collision number between the emulsion droplets. In the last period of experiment, where the retentate contains a large amount of hydrocarbon droplets, oily wall begins to form above the membrane surface and is compacted. Membrane swelling caused by the contact with oily droplet may also have caused the reduction in the flux. Thus, the FD increases with an increase in transmembrane pressure difference. On the other hand, Fig. 10 was showed anti-fouling properties of M1 and M2 against hydrocarbon of bilge water, which was calculated by using Eq. (4). Accordingly, M2 was showed anti-fouler behavior as it is clearly seen in Fig. 10. Believably, successful immobilization and effective back wash solution which was hydrochloric acid and water (1:10) were the main cause of this behavior.

3.4.3 Rejection

The rejection percentage (%R) of hydrocarbons in bilge water after separation process has been calculated by Eq. (2) and is depicted in Fig. 11. It is found that both membranes have more than 90% rejection in all applied pressures. Moreover, the rejection percentage went down as the transmembrane pressure difference increased, sincehigher pressure forced hydrocarbon droplets to pass through the membrane pores and would block the smaller pore after some time. The rejection of M1 was lower than M2, which can be attributed to the higher hydrophilicity and the superior morphological structure in the top- and sub-layer of M2, especially for the oil separation. It is also worth to note that, according to the standard set by the European Union (EU), the oil and grease (source of hydrocarbons) in the wastewater should not be more than 5 mg/L. Hence it can be concluded that the nanocomposite membrane (M2) has met the EU requirement. Ti detection in the permeate water has been checked by using the flame AAS analyzer. The AAS analysis has detected 1.0 ppb of Ti element in treated water, which is considered insignificant.

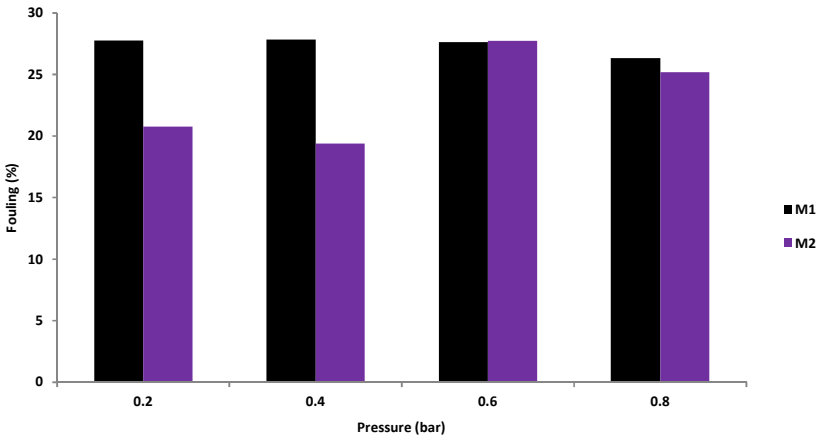

Fig. 9. Fouling after 1 h of operation at different transmembrane pressure differences for M1 (black) and M2 (violet)

RSC Advances Accepted Manuscript

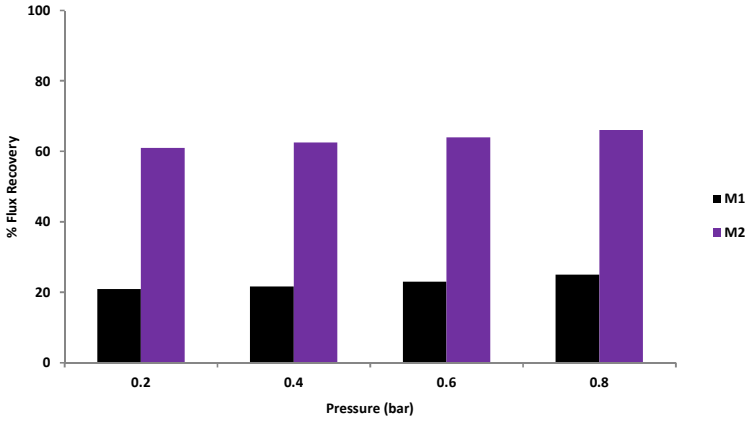

Fig. 10. Flux recovery after 1 h of operation at different transmembrane pressure differences after back wash for M1 (black) and M2 (violet)

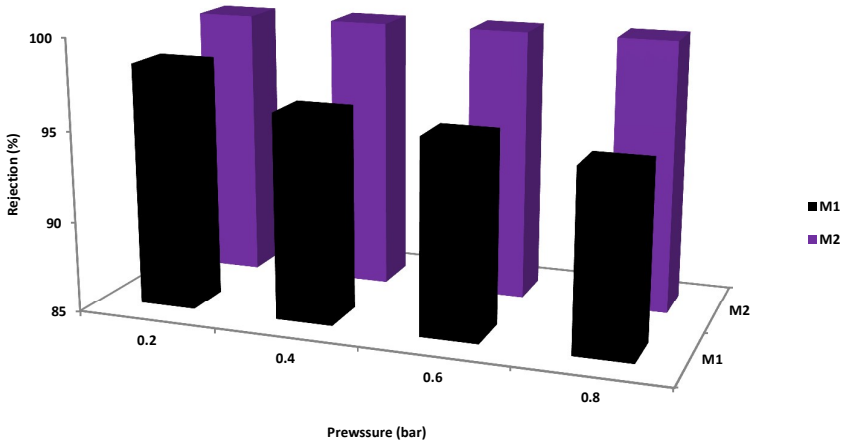

Fig. 11. Rejection of membrane at different transmembrane pressure differences for M1 (black) and M2 (violet)

4.0 Conclusions

Photocatalytic membrane reactor (PMR) was constructed and tested for the photocatalytic degradation and removal of hydrocarbons from bilge water. Neat PVDF membrane (M1) and nanocomposite TiO_2-HNTs/PVDF membrane (M2) were installed in the PMR to know the effect of the incorporation of photocaltalyst TiO_2-HNTs in the PVDF matrix. The performance of the PMR has shown more than 99.9% of hydrocarbon removal from the bilge water when M2 was used. Significant photodegradation and separation efficiency were depicted from the experimental results obtained for M2. It was concluded that TiO_2 immobilization on the surface of HNTs allowed uniform dispersion of the photocalatysts when embedded to the PVDF polymer matrix, showing high photocatalyst activity, reasonable permeation flux and anti-fouling properties. Finally, by the GC-MS analyses of the hydrocarbon concentration in the permeate side, it was found to be below than the standard set by EU.

RSC Advances Accepted Manuscript

Acknowledgement

The authors gratefully acknowledge financial support from the European Commission FP7 - LIMPID (Project number: NMP3-SL-2012-310177) and technical support from both Aquakimia Sdn. Bhd. and Research Management Centre, Universiti Teknologi Malaysia. The authors also acknowledge Solvay Specialty Polymers Italy and Johnson Matthey PLC UK for providing materials used in this work.

References

1. D. Cazoir, L. Fine, C. Ferronato and J. M. Chovelon, *J Hazard Mater*, 2012, **235-236**, 159-168.
2. B. Chakrabarty, A. K. Ghoshal and M. K. Purkait, *Journal of Membrane Science*, 2008, **325**, 427-437.
3. B. Yildiz and M. S. Kazimi, *International Journal of Hydrogen Energy*, 2006, **31**, 77-92.
4. F.-q. Lin, S.-f. LIN and S.-b. ZENG, *Ship Science and Technology*, 2009, **5**, 036.
5. K. Oshima, J. Kajiyama and S. Fukumoto, US Patent 3,617,566, 1971.
6. L. Kerambrun and G. Peigné, International Oil Spill Conference, 1991.
7. G. T. Tellez, N. Nirmalakhandan and J. L. Gardea-Torresdey, *Microchemical journal*, 2005, **81**, 12-18.
8. B. K. Körbahti and K. Artut, *Desalination*, 2010, **258**, 219-228.
9. M. Nievas, M. Commendatore, N. Olivera, J. Esteves and V. Bucala, *Bioresource technology*, 2006, **97**, 2280-2290.
10. N. Bailey, A. Jobson and M. Rogers, *Chemical geology*, 1973, **11**, 203-221.
11. M. Lu, Z. Zhang, W. Yu and W. Zhu, *International Biodeterioration & Biodegradation*, 2009, **63**, 316-321.
12. M. Pacwa-Płociniczak, G. A. Płaza, Z. Piotrowska-Seget and S. S. Cameotra, *International journal of molecular sciences*, 2011, **12**, 633-654.
13. S. Patsios, V. Sarasidis and A. Karabelas, *Separation and Purification Technology*, 2013, **104**, 333-341.
14. S. Mozia, *Separation and Purification Technology*, 2010, **73**, 71-91.
15. M. N. Chong, B. Jin, C. W. Chow and C. Saint, *Water research*, 2010, **44**, 2997-3027.
16. M. Bayati, F. Golestani-Fard and A. Moshfegh, *Catalysis letters*, 2010, **134**, 162-168.
17. X. He, Y. Cai, H. Zhang and C. Liang, *J. Mater. Chem.*, 2010, **21**, 475-480.
18. J. Zhao, K. Wu, T. Wu, H. Hidaka and N. Serpone, *J. Chem. Soc., Faraday Trans.*, 1998, **94**, 673-676.
19. J. Saien and H. Nejati, *J Hazard Mater*, 2007, **148**, 491-495.
20. B. Chakrabarty, A. K. Ghoshal and M. K. Purkait, *Chemical Engineering Journal*, 2010, **165**, 447-456.
21. L. G. Devi and B. N. Murthy, *Catalysis letters*, 2008, **125**, 320-330.
22. P. Stepnowski, E. Siedlecka, P. Behrend and B. Jastorff, *Water research*, 2002, **36**, 2167-2172.
23. W. Oh and M. Chen, *Bulletin-Korean Chemical Society*, 2008, **29**, 159.
24. X. Pan, Y. Zhao, S. Liu, C. L. Korzeniewski, S. Wang and Z. Fan, *ACS applied materials & interfaces*, 2012, **4**, 3944-3950.
25. E. Bae and W. Choi, *Environmental science & technology*, 2003, **37**, 147-152.
26. R. Wang, G. Jiang, Y. Ding, Y. Wang, X. Sun, X. Wang and W. Chen, *ACS Appl Mater Interfaces*, 2011, **3**, 4154-4158.

RSC Advances Accepted Manuscript

27. S. A. Hashemifard, A. F. Ismail and T. Matsuura, *Journal of colloid and interface science*, 2011, **359**, 359-370.
28. Y. Chen, Y. Zhang, J. Liu, H. Zhang and K. Wang, *Chemical Engineering Journal*, 2012, **210**, 298-308.
29. Y. Zhang, Y. Chen, H. Zhang, B. Zhang and J. Liu, *Journal of inorganic biochemistry*, 2013, **118**, 59-64.
30. X. Gao, P. W. Huo, X. L. Liu, D. Wu, Z. Y. Lu and Y. S. Yan, *Applied Mechanics and Materials*, 2013, **316**, 1041-1044.
31. L.-Y. Yu, H.-M. Shen and Z.-L. Xu, *Journal of Applied Polymer Science*, 2009, **113**, 1763-1772.
32. S. Singh, K. Khulbe, T. Matsuura and P. Ramamurthy, *Journal of Membrane Science*, 1998, **142**, 111-127.
33. A. F. Ismail, S. A. Hashemifard and T. Matsuura, *Journal of Membrane Science*, 2011, **379**, 378-385.
34. M. Vela, S. Á. Blanco, J. L. García and E. B. Rodríguez, *Separation and purification Technology*, 2008, **62**, 489-498.
35. N. Ochoa, M. Masuelli and J. Marchese, *Journal of Membrane Science*, 2003, **226**, 203-211.

RSC Advances Accepted Manuscript